A 3-D Organically Synthesized Porous Carbon

Ziqiang Zhao,[a] Saikat Das,[a] Guolong, Xing,[a] Pierre Fayon,[b] Patrick Heasman,[b] Michael Jay,[b] Steven Bailey,[b] Colin Lambert,[b] Hiroki Yamada [c], Toru Wakihara,[c] Abbie Trewin,*[b] Teng Ben,*[a] Shilun Qiu[a], Valentin Valtchev[a,d]

Abstract: We report the first organically synthesized *sp-sp*^{3} hybridized porous carbon. OSPC-1, this new carbon, shows electron conductivity, high porosity, the highest uptake of lithium ions of any carbon material to-date and the ability to inhibit dangerous lithium dendrite formation. The new carbon exhibits exceptional potential as anode material for lithium-ion batteries (LIBs) with high capacity, excellent rate capability, long cycle life and potential for improved safety performance.

In recent years porous carbon has reaped pronounced importance to the scientists because of special advantages like amazing surface areas, very high pore volumes etc.[1] as these materials can find many applications that cover electron conduction and storage,[2] catalysis,[3] separation etc.[1] Porous carbon has also been used largely as electrode in lithium-ion batteries (LIBs).[4-8] Physical and chemical activation techniques are ordinarily used to form activated carbons.[4,9] Synthesis of porous carbons to use templates like zeolites, inorganic material etc. is alternate method. Ordered microporous carbon with high specific surface areas taking zeolites as templates have been synthesized by Kyotani *et al*.[10] There are two prevailing methods i.e. hard template and soft template methods to form ordered mesoporous carbons.[2] Ryoo *et al.* developed ordered mesoporous carbon using mesoporous silica molecular sieves as template.[11] Carbide-derived carbon is developed after removal of metal or metalloid from carbide.[12] Notwithstanding all these prevailing methods use carbonization, template method, arc-dischrge or laser ablation[2b] to form porous carbon and there is no organic synthesis method so far to form porous carbon. As yet porous carbon cannot be designed on a molecular level.

On the other hand, covalent organic frameworks (COFs)[13a] and metal organic frameworks (MOFs)[13b] are developed by designing of structral building uints first and then developed into a network. But porous carbon has not been synthesized yet following this technique. This prompted us to perform the design of structural building units and form a carbon network. Herein we specially design the structural building units, ethynyl methane[14] to form three dimensional connected carbon network, polytetraethynylmethane (OSPC-1). In this paper we describe for the first time the organic synthesis of a new 3-D porous carbon by Eglinton homocoupling.[15] This porous carbon prepared is also the first *sp-sp*^{3} hybridized carbon combined with electron conductivity, high porosity and high lithium ions uptake.

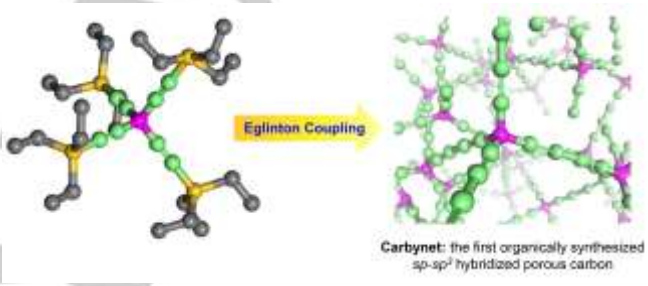

Figure 1. Reaction scheme to form OSPC-1 and 3D structure of OSPC-1. Violet: *sp*^{3} carbon, green: *sp* carbon, yellow: silicon, grey spheres represent carbon atoms in the TES protecting groups of the starting material, H atoms are omitted for clarify.

OSPC-1 was synthesized via a catalytic Eglinton homocoupling of ethynyl methane, shown in Figure 1. The full synthetic procedure with the corresponding schemes are outlined in Supplementary Materials. The XRD analysis of OSPC-1 shows that the resulting material is amorphous in nature (Figure S1). From XPS analysis of OSPC-1 (Figure 2a), we can see a C 1*s* peak at 285 eV with a shoulder towards higher energies. The peak is deconvoluted into three peaks at 284.5 eV, 285.8 eV and 288.4 eV, peak at 284.5 eV is assigned to carbon with *sp*^{3} hybridization and peak at 285.8 eV is assigned to carbon with *sp* hybridization.[16] Carbon with *sp*^{2} hybridization appear at 285.05 eV is absent in the spectra.[16,17] The ratio of C(*sp*) to C(*sp*^{3}) is 5:2 differs from the expected value of 8:1, can be attributed to the higher stability of C(*sp*^{3}) at the surface as XPS is a surface specific technique. Besides, XPS spectra of OSPC-1 synthesized in a glove box shows peak at 288.4 eV assigned to carbon bonded to oxygen is reduced from 20% to 14.5%, confirms that the surface carbon is terminated with oxygen atoms.[18-20] Notably, in OSPC-1 the conjugation is broken by *sp*^{3} carbon, so only the terminal alkynyl is highly reactive to oxygen.

After analysis of the solid state NMR of OSPC-1 (Figure S3) two peaks can be observed at 133 and 53 ppm that can be assigned to C(*sp*) and C(*sp*^{3}), respectively. Broad nature of peaks suggests low symmetry of the amorphous framework. From EDS analysis, impurities in OSPC-1 is below 1% (Figure S4), similarly to high purity diamond, graphite or graphene. Presence of

[a] Z. Zhao, S. Das, Prof. T. Ben, Prof. S. Qiu, Prof. V. Valtchev
Department of Chemistry
Jilin University
130012 Changchun China
E-mail: tben@jlu.edu.cn

[b] Dr. P. Fayon, P. Heasman, M. Jay, S. Bailey, Prof. C. Lambert, Dr. A. Trewin
Department of Chemistry and Physics
Lancaster University
Bailrigg, Lancaster, UK, LA1 4YB
E-mail: a.trewin@lancaster.ac.uk

[c] H. Yamada, Prof. T. Wakihara
Department of Chemical System Engineering
The University of Tokyo
Tokyo, JP, 113-8656

[d] Prof. V. Valtchev
Laboratoire Catalyse & Spectrochimie
Université de Caen-ENSICAEN-CNRS
Caen, France

Supporting information for this article is given via a link at the end of the document.

carbon-carbon triple bonds with a peak at 2150 cm^{-1} (Figure S5) is proved from the FT-IR analysis.[21] OSPC-1 show good stability up to 420 °C in N_2 atmosphere (Figure S 6). After analysis of Raman spectrum of OSPC-1, we find broad peak at 1363 cm^{-1} assigned to the carbon-carbon single bond, weak peak at 2094 cm^{-1} assigned to the carbon-carbon triple bond, peak at 1588 cm^{-1} assigned to the bends and stretches within the C(sp^3)-C(sp)-C(sp)-C(sp)-C(sp)-C(sp^3), detailed explanation can be found in Supporting Information section 7. EELS of OSPC-1 (Figure 2b) exhibits peaks at 285.8 eV and 292.8 eV attributed to *sp* and sp^3 carbon respectively, however it shows no sp^2 peak which proves that OSPC-1 is composed of *sp* and sp^3 carbon only.[22-26].

In the next step pair distributions were carried out to compare models to experiment for amorphous carbons.[27,28] Pair distribution function, *G*(*r*), of the OSPC-1 is obtained from total structure factor, *S*(*Q*), C-C correlations are similar to those observed for graphite, fullerene, and carbon nanotubes (Figure S15). However, OSPC-1 shows an additional *G*(*r*) peak at ~3.1 Å, which is exclusive in case of OSPC-1 and not found in other carbon materials. From the pair distribution function clear proof of the unique nature of the new carbon that is built up from linked C(*sp*) and C(sp^3) is provided.

Next we generated structural models of OSPC-1 using our in-house developed *Ambuild* code[29] for the purpose of rationalizing the amorphous 3D nature of OSPC-1. The details on computation and images of models are shown in Supporting Information. Crystalline forms of OSPC-1 are possible e.g. with **dia** or **qtz** topology (Figure S17-S18), these require reversible chemistry to form but not possible within present synthetic strategy. Amorphous non-interpenetrated structure of OSPC-1 is confirmed from the models. Flexibility of the ethynyl strut between sp^3 carbon nodes contributes to the amorphous nature. Fragments of the resulting models (Figure S24) illustrate the flexibility within structure arises from small deviations of the C(sp^3)–C(sp)–C(sp) angle. Radial distributions calculated for all carbon atoms for Models-1-5 are shown in Figure S26-S30, and a number of peaks that correlate well with experimental radial distribution, including the peak at ~3.1 Å, which is attributed to the C(*sp*) to C(*sp*) on adjacent ethynyl struts (Figure 2c).

Following the assessment of the nitrogen uptake isotherm at 77 K, OSPC-1 is found to be microporous in nature with a SA_{BET} = 766 $m^2\ g^{-1}$. As seen the isotherm is close to type II with substantial uptake at low relative pressure showing substantial presence of micropores. From TEM inspection (Figure 2d) of OSPC-1 we find that worm-like pores exist and no graphite ribbons are seen. Using QSDFT analysis, pore size distribution derived from the nitrogen uptake isotherm[30] gives peaks centered at 1.0 and 2.3 nm (Figure S33-S34). After this, the solvent accessible surface areas for the models were calculated using a probe radius of 1.82 Å (the kinetic radius of nitrogen) giving a range between 731 and 784 $m^2\ g^{-1}$ (Table S2) which show good agreement with experimental result. The calculated pore size distributions also match well with the experimental data (Figure S35).

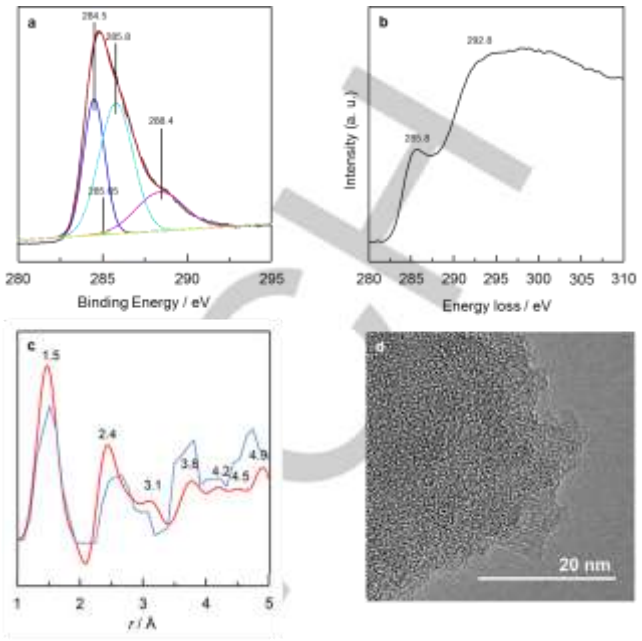

Figure 2. (a) Fitted C1s XPS spectra of OSPC-1. (b) Electron energy loss spectra of OSPC-1. (c) The reduced pair distribution function, *G*(*r*), of OSPC-1 (red: observed, blue: simulated). (d) High resolution TEM of OSPC-1.

With reference to electron conduction, graphene and graphite reveal exceptional electron conduction with conductivity of 1.00 × 10^{10} S cm^{-1} and 2.00 × 10^7 S cm^{-1}, respectively. Direct electron conduction pathway is provided by the highly delocalised orbitals of sp^2 hybridized carbon-carbon bonding. Again, diamond with highly localised sp^3 hybridization is an insulator (conductance is 1.00 × 10^{-11} S cm^{-1}). OSPC-1 in this work combines conjugated *sp* and non-conjugated sp^3 hybridized carbon atoms is not expected to be conductive as the electron conduction pathways will be blocked by the non-conjugated sp^3 hybridized carbon atoms. However we found the conductivity of OSPC-1 to be high (σ = 1.2 × 10^{-4} S cm^{-1}) as determined from the Nyquist plot (Figure S36).

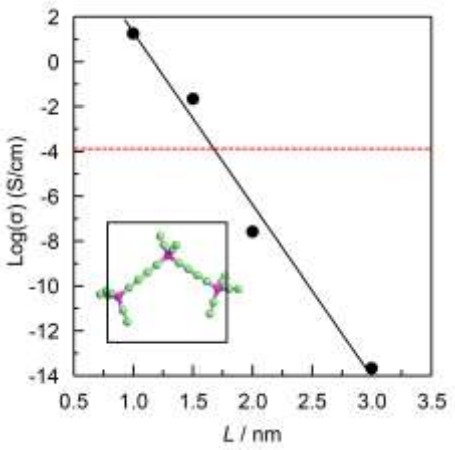

Figure 3. The log of the ensemble averaged conductivity$\sigma(L)$ obtained from the average conductance of cubes of OSPC-1 of size L (black). Dashed line denotes the experimentally measured value as $\sigma = 1.2 \times 10^{-4}$ S cm^{-1}. Inset shows a cube of 1.7 nm with a representative OSPC-1 fragment.

OSPC-1 is an amorphous 3D structure and it therefore needs a novel approach to assess the conduction pathways and transport properties by using tight binding (TB) transport calculations or density functional theory (DFT) calculations and the details of these methods are presented in the Supporting Information section 13. OSPC-1 is a disordered wide band gap semiconductor at length scales less than the inelastic mean free path λ, suggests that electron transport takes place by phase-coherent tunneling and therefore the conductivity, σ should be obtained by computing the ensemble averaged conductance G of random cubes of OSPC-1 using the relation $\sigma = G/\lambda$ to analyze the results. λ is an unknown quantity, the ensemble-averaged conductance $G(L)$ for cubes of various size L is computed and the quantity $\sigma(L) = G(L)/L$ is plotted versus L (Figure 3). The experimental conductivity (dashed line) coincides with $\sigma(L)$ at a length scale λ= 1.7 nm. Free path is on the scale of the size of the OSPC-1 fragment (Figure 3). The DFT calculations qualitatively reinforce the TB calculations with agreement of the equivalent peak positions for the highest occupied molecular orbital (HOMO) and lowest unoccupied molecular orbital (LUMO) levels in respective density of states (DOS) plots (Figure S43-S44). Wavefunction analysis shows conduction pathways along the chain lengths which is particularly apparent at the energies associated with the HOMO (H1) and LUMO (L0 and L1) levels (Figure S45).

Graphite is common anode material for lithium ion batteries but swelling upon lithium ions causes fractures and ultimately destroy the crystal structure, which is the main reason for the short lifetime of the battery. Besides this, lithium dendrites can develop at the graphite-electrolyte interface extend towards the cathode which results in a short circuit even explosion. Thus we can see that new carbon materials with stable lithium ion uptake are an attractive option.

A reversible lithium ion capacity of OSPC-1 of 748 mAh g^{-1} is obtained at a current density of 200 mA g^{-1} after 100 cycles, therefore suggest that the reversible capacity of OSPC-1 surpasses C_{60} (2.5 mAh g^{-1}), CNTs (224 mAh g^{-1}) and graphite (324 mAh g^{-1}) under the same condition (Figure 4a, Figure S47-S49). The voltage profiles (Figure S50) of OSPC-1 show a different lithium insertion/extraction mechanism to graphite.[31] No distinguishable plateaus are observed in the slope, suggesting that electrochemical and geometrically nonequivalent Li ion sites exist, consistent with the CV curves (Figure S51).

An average simulated capacity of lithium ion uptake (Figure 4b) within the microporous region of OSPC-1 of 491 mAh g^{-1} is calculated for the OSPC-1 models using simulated annealing, shown in Supplementary Materials Table S4. The total capacity of 786 mAh g^{-1}, based upon the ratio of volume within the microporous and mesoporous regions obtained from analysis of the nitrogen uptake isotherm is in excellent agreement with experimental value. Molecular dynamic (MD) simulations is used to assess the ability of lithium ions to diffuse through the OSPC-1 structure. Lithium ions diffuse freely through the microporous regions of the Model-1a OSPC-1 structure with a diffusion coefficients of ~4 × 10^{-4} cm^2 s^{-1}, which is similar to values determined for lithium ion diffusion in polyelectrolyte solutions[32]. Full computational details are shown in Supporting Information section 15.2.

Then overcharge experiments are carried out to determine the high cycling stability of OSPC-1 anode compared to graphite anode. SEM results show that no dendrites are developed on the surface of OSPC-1 (Figure 4c), while dendrites are largely present on the graphite surface under similar conditions (Figure 4d). The XRD patterns of the cells after 100 cycles at a current density of 200 mA g^{-1} do not show formation of a lithium crystalline phase (Figure S65). This result reveals the high resistance of OSPC-1 to the formation of hazardous dendrites, which is assigned to the three-dimensional porous network of this exceptional material. The rate capability of OSPC-1 with various current densities from 100 to 3000 mA g^{-1} shows that even at high current density of 1000, 2000 and 3000 mA g^{-1}, there are still reversible capacities of 530, 416 and 356 mAh g^{-1} after 10 cycles, respectively. When the current density is reset to 100 mA g^{-1}, capacity increases back to 944 mAh g^{-1} (Figure 4e). Capacity against current density for OSPC-1 compared to carbon materials (Figure 4f) proves the uniqueness of OSPC-1.

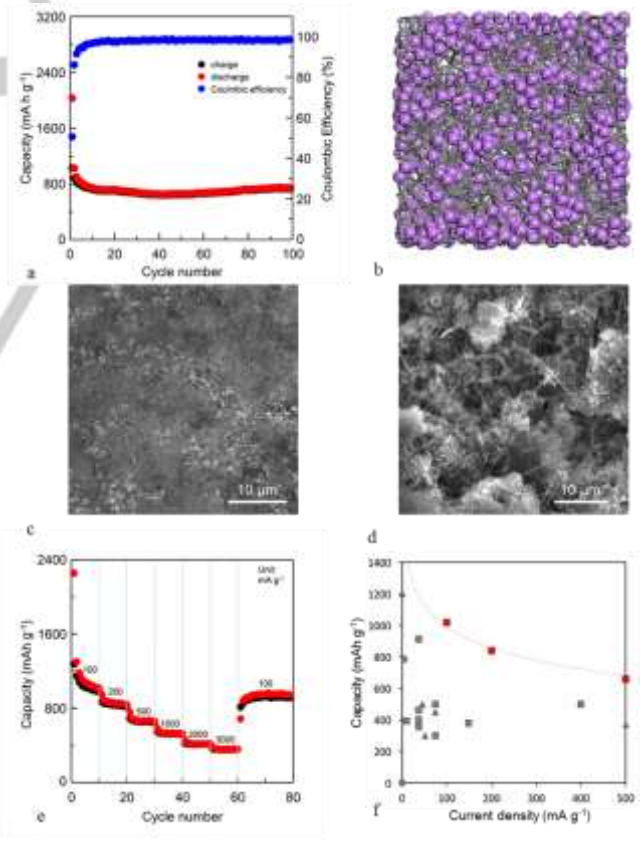

Figure 4. (a) Cycling performance of OSPC-1 showing the discharge capacity (red symbols) and charge capacity (black symbols) at a current density of 200 mA g^{-1} for 100 cycles; Blue symbols: coulombic efficiency. (b) The simulated capacity of lithium ions within Model-1a. (c) SEM image of OSPC-1 after overcharge at a current density of 5000 mA g^{-1} for 6 min. (d) SEM image of graphite after overcharge under similar condition. (e) Rate capability with

various current densities from 100 to 3000 mA g^{-1} of OSPC-1. (f) Capacity against current density for carbon materials (grey) compared to OSPC-1 (red).

In summary, we reportedly demonstrate an organic synthetic strategy to attain porous carbon (OSPC-1) which is entirely different from the prevailing methods to prepare porous carbon thereby favoring the design of porous carbon on molecular level. This material is the only porous carbon that is constructed from *sp* and sp^3-hybridized carbon. Furthermore, we have demonstrated that OSPC-1 is a highly promising anode material for LIBs with high capacity, impressive rate capability, long cycle life and the potential for improved safety performance. The synthetic method, which is based upon versatile organic polymerization, has potential to be extended to other 3D carbon materials and thus spreads out the research frontiers to a new family of porous carbon materials.

Acknowledgements

AT acknowledges the Royal Society. This work was supported by the NSFC (Grant no.21390394, 21471065), the "111" project (B07016). CJL is supported by EPSRC projects EP/N017188/1, EP/M014452/1, EP/P027156/1. VV acknowledges the Thousand Talents program (china) for support and the NSFC (no. 21571078). TB, SQ and VV acknowledge the support in the framework of China-French joint laboratory "Zeolites". The synchrotron radiation experiments were performed at the BL04B2 in the SPring-8 with the approval of the Japan Synchrotron Radiation Research Institute (JASRI) (Proposal Number 2017A0115).

Keywords: carbon • amorphous materials • semiconductors • synthesis design • conducting materials

[1] B. Sakintuna, Y. Yürüm, *Ind. Eng. Chem. Res.* **2005**, *44*, 2893-2902.
[2] a) M. R. Benzigar, S. N. Talapaneni, S. Joseph, K. Ramadass, G. Singh, J. Scaranto, U. Ravon, K. A. Bahily, A. Vinu, *Chem. Soc. Rev.* **2018**, *47*, 2680-2721; b) A. D. Roberts, X. Li, H. Zhang, *Chem. Soc. Rev.* **2014**, *43,* 4341-4356.
[3] C. Zhu, H. Li, S. Fu, D. Du, Y. Lin *Chem. Soc. Rev.* **2016**, *45*, 517-531.
[4] W. Long, B. Fang, A. Ignaszak, Z. Wu, Y. Wang, D. Wilkinson, *Chem. Soc. Rev.* **2017**, *46*, 7176-7190.
[5] A. M. Stephan, T. P. Kumar, R. Ramesh, S. Thomas, S. K. Jeong, K. S. Nahm, *Mater. Sci. Eng. A.* **2006**, *430*, 132-137.
[6] Y. J. Hwang, S. K. Jeong, K. S. Nahm, J. S. Shin, S. A. Manuel, *J. Phy. Chem. Solids* **2007**, *68*, 182-188.
[7] Y. S. Hu, P. Adelhelm, B. M. Smarsly, S. Hore, M. Antonietti, J. Maierm, *Adv. Funct. Mater.* **2007**, *17*, 1873-1878.
[8] S. H. Yeon, K. N. Jung, S. Yoon, K. H. Shin, C. S. Jin, *J. Phys. Chem.Solids* **2013**, *74*, 1045-1055.
[9] a) M. M. Titirici, M. Antonietti, *Chem. Soc. Rev.* **2010**, *39*, 103-116; b) P. Kalyani, A. Anitha, Int. J. Hydrogen Energy, **2013**, *38*, 4034-4045.
[10] a) Z. X. Ma, T. Kyotani, A. Tomita, Chem. Commun. **2000**, *23*, 2365-2366; b) H. Nishihara, T. Kyotani, *Adv. Mater.* **2012**, *23*, 4473-4498.
[11] R. Ryoo, S. H. Joo, S. Jun, *J. Phys. Chem. B* **1999**, *103*, 7743-7746.
[12] a) G. N. Yushin, E. N. Hoffman, A. Nikitin, H. Ye, M. W. Barsoum, Y. Gogotsi, *Carbon*, **2005**, *43*, 2075-2082; b) V. Presser, M. Heon, Y. Gototsi, *Adv. Funct. Mater.* **2011**, *21*, 810-833.
[13] a) P. J. Waller, F. Gándara, O. M. Yaghi, *Acc. Chem. Res.* **2015**, *48*, 3053-3063; b) A. Schoedel, M. Li, D. Li, M. O'Keeffe, O. M. Yaghi, *Chem. Rev.* **2016**, *116,* 12466-12535.
[14] R. Amemiya, K. Suwa, J. Toriyama, Y. Nishimura, M. Yamaguchi, *J. the Am. Chem. Soc.* **2005**, *127*, 8252-8253.
[15] G. Eglinton, A. R. Galbraith, *J. Chem. Soc.* **1959**, *182*, 889-896.
[16] Y. X. Shao, Y. H. Cai, D. Dong, S. Wang, G. A. Siau, G. Q. X, *Chem. Phys. Lett.* **2009**, *482*, 77-80.
[17] F. Tao, M. Qiao, Z. Li, L. Yang, J. Yu, G. Hai,Q. Guo, *Phys. Rev. B* **2003,** *67*, 115334.
[18] P. Zabek, J. Eberl, H. Kisch, *Photochem. Photobiol. Sci.* **2009**, *8,* 264-269.
[19] D. Chen, Z. Jiang, J. Geng, Q. Wang, D. Yang, *Ind. & Eng. Chem. Res.* **2007**, *46*, 2741-2746.
[20] Y. Taki, O. Takai, *Thin Solid Films* **1998,** *316*, 45-50.
[21] M. Häussler, R. Zheng,W. Y. Lam, H. Tong, H. Dong, B. Tang, *J. Phys. Chem. B* **2004,** *108*, 10645-10650.
[22] A. Dato, V. Radmilovic, Z. H. Lee, J . Philips, M. Frenklach, *Nano Lett.* **2008**, *8,* 2012-2016.
[23] P. K. Chu, L. H. Li, *Mater. Chem. Phys.* **2006,** *96,* 253–277.
[24] A. D. Moller, F. E. Magaña, R. M. Sanchez, M. A. Borja, G. A. Hirata, L. C. Araiza, *J. Electron. Spectrosc. Relat. Phenom.* **1999,** *104,* 61-66.
[25] A. P. Hitchcock, S. Johnston, T. Tyliszczak, C. C. Turci, M. Barbatti, A. B. Rocha, C. E. Bielschowsky, *J. Electron. Spectrosc. Relat. Phenom.* **2002**, *123,* 303-314.
[26] V. Mortet, L. Zhang, M. Eckert, J. D`Haen, A. Soltani, M. Moreau, D. Troadec, E. Neyts, J. D. Jaeger, J. Verbeeck, A. Bogaerts, G. V. Tendeloo, K. Haenen, P. Wagner, Phys. *Status Solidi A* **2012,** *209,* 1675-1682.
[27] S. K. Jain, R. J. M. Pellenq, J. P. Pikunic, K. E. Gubbins, *Langmuir* **2006,** *22*, 9942-9948.
[28] P. Kowalczyk, A. P. Terzyk, P. A. Gauden, S. Furmaniak, M. Wisniewski, A. Burian, L. Hawelek, K. Kaneko, A. V. Neimark, *J. Phys. Chem. C* **2014,** *118,* 12996-13007.
[29] J. M. H. Thomas, A. Trewin, *J. Phys. Chem. C* **2014,** *118,* 19712-19722.
[30] M. S. José, A. Emilio, D. G. Julian, G. Alberto, J. Javier, O. Pablo, S.-P. Daniel, *J. Phys.: Condens. Matter* **2002,** *14,* 2745.
[31] a) S. Megahed, J. Power Sources, **1994**, *51*, 79-104; b) S. Flandrois, B. Simon, Carbon, **1999**, *37*, 165–180.
[32] H. G. Buss, S. Y. Chan, N. A. Lynd, B. D. McCloskey, *ACS Energy Lett.* **2017**, *2,* 481-487.

Entry for the Table of Contents

Layout 1:

COMMUNICATION

The first 3-D sp-sp^3 hybridized porous carbon material prepared by organic procedure with high conductivity.

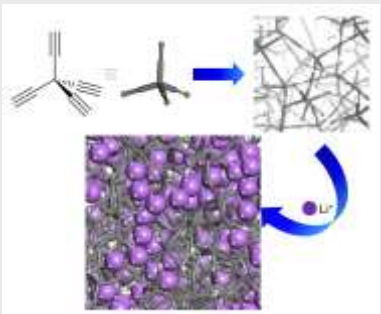

Z. Zhao,[a] S. Das,[a] G. Xing,[a] P. Fayon,[b] P. Heasman,[b] M. Jay,[b] S. Bailey,[b] C. Lambert,[b] H. Yamada[c], T. Wakihara,[c] A. Trewin,[b] T. Ben,*[a] S. Qiu[a], V. Valtchev[a,d]*

Page No. – Page No.

A 3-D Organically Synthesized Porous Carbon